LANGMUIR

Article

pubs.acs.org/Langmuir

Nanoridge Formation and Dynamics of Stratification in Micellar Freestanding Films

Yiran Zhang and Vivek Sharma*

Department of Chemical Engineering, University of Illinois at Chicago, Chicago, Illinois 60607, United States

Supporting Information

ABSTRACT: Controlling and predicting the stability and lifetime of freestanding films, including foam and emulsion films, is crucial for many industrial and biological applications. Freestanding films (thickness <100 nm), stabilized by surfactants above the critical micelle concentration, exhibit stratification or stepwise thinning. Stratification proceeds by formation of thinner domains that grow at the expense of surrounding films. In this Article, we address several long-standing challenges related to the experimental characterization and theoretical description of thickness variations, forces, fluxes and flows underlying stratification. We show that nanoridges form and grow at the moving front around expanding domains, and we visualize their shape evolution using Interferometry Digital Imaging Optical Microscopy (IDIOM) protocols with an unprecedented spatiotemporal resolution (thickness <10 nm, time <1 ms). We develop a theoretical model for drainage via stratification under the influence of supramolecular oscillatory surface forces arising from the confinement-induced layering of micelles, and we show that the nanoridge growth and domain expansion dynamics can be modeled quantitatively.

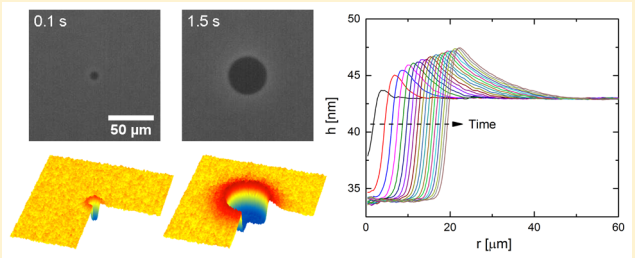

The fluxes, forces, and flows that drive drainage and rupture of freestanding films determine the stability, lifetime, properties and applications of soap bubbles,[1,2] lipid films and bilayers,[2] and colloidal dispersions,[3] including foams and emulsions. The influence of thin films on physicochemical properties and shelf life of colloidal dispersions can be visualized most easily for foams. Foams comprise gas pockets dispersed in a three-dimensional network of thin liquid films and thicker Plateau borders (channels and nodes) formed by their intersections.[3−5] Standard models of film drainage that account for capillary suction into the Plateau borders and viscous (interfacial and bulk) resistance, predict a monotonic decrease in thickness of plane-parallel films.[4−7] However, many ultrathin films of soft matter exhibit stratification, manifested as stepwise thinning in the interferometry-based measurements of average film thickness.[8−16] In reflected light microscopy, stratifying films display regions with distinct colors or shades of gray[2,3,7−16] implying that domains and nanostructures with discretely different thickness form and coexist in the thinning film. Stratification is attributed to confinement-induced layering of supramolecular structures like micelles,[8−13,15] nanoparticles,[8,9,11,14,17] polyelectrolytes[14] and smectic mesophases.[16] However, visualization and characterization of nanoscopic thickness transitions and variations, as well as their theoretical description, remain longstanding, unresolved challenges, and are addressed in this contribution, for stratifying micellar freestanding films formed with surfactants above their critical micelle concentration (CMC).

In ultrathin films (h < 100 nm), when the two interfacial regions approach each other, intermolecular and surface forces contribute a thickness-dependent disjoining pressure[18−20] that can enhance or reduce the drainage rate, and even counterbalance the capillary pressure. Historically, though Newton, Hooke, and Brewster had noted that drainage of soap films continues until relatively a stable black film emerges,[1,4] the critical role of disjoining pressure, was outlined first by Derjaguin and co-workers[18] in the 1940s. Hydrodynamics in relatively thin films (thickness, h < 20 nm) including soap films[21−24] is dependent on the same contributions to disjoining pressure resulting from overlapping electrostatic double layers, electromagnetic fluctuation fields, and adsorbed layers (of surfactants or polymers) that are often used for describing colloidal stability.[18,20,25] In the early twentieth century, Johonnott[26] and Perrin[27] reported both stepwise thinning and thickness inhomogeneity in relatively thicker soap films (h > 20 nm). Relatively recent papers[11,14] argue that a less-well understood, structural contribution to disjoining pressure drives stratification in ultrathin films of simple liquids[20,24,25,28] and of soft matter containing supramolecular structures like micelles, nanoparticles, and polyelectrolytes.[11,14,16] The structural contribution that arises due to layering of supramolecular structures is referred to hereafter as the supramolecular oscillatory structural force contribution. In micellar freestanding films, amphiphilic molecules populate the fluid−fluid interfaces and self-assemble to form micelles in the bulk liquid.[20] Thus, in

Special Issue: Early Career Authors in Fundamental Colloid and Interface Science

Received: June 3, 2017
Revised: July 26, 2017
Published: July 28, 2017

DOI: 10.1021/acs.langmuir.7b01871
Langmuir XXXX, XXX, XXX−XXX

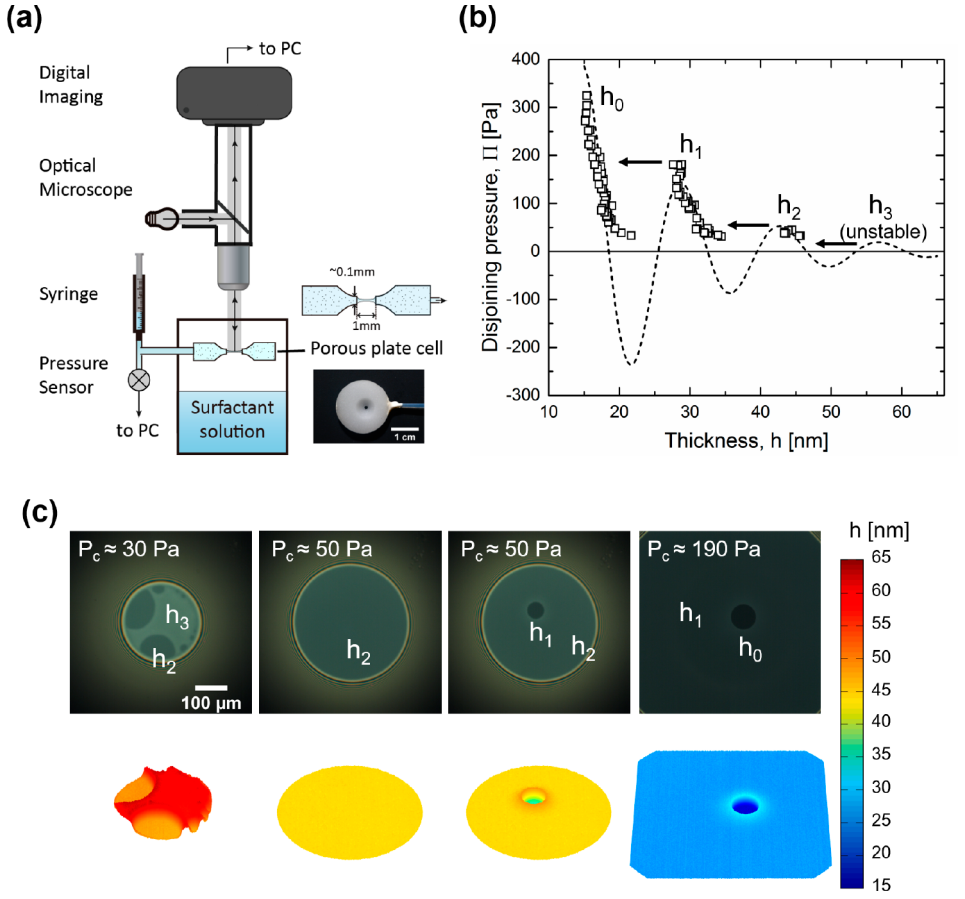

Figure 1. Disjoining pressure isotherm and stratification in thin films made from micellar, 50 mM SDS solution. (a) Schematic of the Interferometry Digital Imaging Optical Microscopy (IDIOM) setup used for quantifying thickness h (x,y,t) variations and transitions within a micellar film undergoing drainage via stratification, and also for measuring the disjoining pressure isotherm. The IDIOM protocols that result in pixel-wise thickness detection, are based on measurement of spatiotemporal variation in interference intensity I (x,y,t) and utilize the photosensor array of a digital camera. (b) Oscillatory disjoining pressure isotherm, Π versus h, measured experimentally for three metastable thickness branches (h_0, h_1, h_2), is shown in hollow squares. For a decaying oscillation function, shown as a dashed line, the period of oscillation is Δh = 13 nm, which is close to the stratification step size, Δh = 13.5 nm. The outermost branch h_3 is observed (see panel c) but is not stable under the experimentally accessible range of pressure ($P_c \geq 30$ Pa). The arrows indicate the pressure at which the transition from a thicker to a thinner branch takes place. (c) Snapshots during the transitions between thickness steps. Darker (thinner) layers grow as single or multiple circular domains in the brighter (thicker) layers. The change in the overall film size is a result of change in applied pressure P_c. For P_c = 50 Pa, representative homogeneous film used for equilibrium disjoining pressure measurement is also shown. Color-coded thickness maps constructed using the IDIOM method show the sharp contrast between regions with discretely different thickness.

addition to the physicochemical properties of interfacially adsorbed surfactants, micellar size and interactions determine the magnitude of capillary suction forces, viscous resistance and disjoining pressure, and must be accounted for in any theoretical analysis of the stratification dynamics.

Stratification proceeds by the formation and growth of one or more thinner, darker domains that expand at the cost of the surrounding thicker film.[8−10,15,29−31] Mechanisms underlying thickness transitions and variations during stratification in micellar films are still under debate.[8−10,15,29−32] Two competing phenomenological models—osmotic-diffusive and hydrodynamic—have been proposed for describing the $R \propto t^{1/2}$ scaling observed during expansion of "isolated" domains, i.e., domains not interacting with each other or with the Plateau border.[10,15,31−33] In the osmotic-diffusive model proposed by Kralchevsky et al.,[10] stratification involves a layer-wise removal of micelles due to diffusion of vacancies from Plateau border into the film. By contrast, Bergeron et al.[29] proposed a hydrodynamic model, in which the $R \propto t^{1/2}$ scaling is a result of an outward radial flow within the inhomogeneous films driven by radial pressure gradients arising due to curvature variation. The $R \propto t^{1/2}$ scaling, associated with a constant apparent diffusivity, is also observed during expansion of isolated domains in films formed with nanoparticle dispersions and solutions of polyelectrolyte−surfactant complexes. For such films, Heinig et al.[31] also developed a hydrodynamic model, suggesting that the $R \propto t^{1/2}$ scaling for domain expansion as well as rim formation are driven by local film tension gradients. However, we recently discovered[15] a second regime with $R \propto t$ scaling is exhibited after domains coalesce with the Plateau border. Constant velocity expansion that was neither reported in experimental studies,[7−11,14,29−31] nor analyzed or anticipated by the aforementioned models.[10,29−32] The constant velocity expansion is also observed after a topological instability creates thicker white spots (or mesas) near the moving front.[15,30,34,35] Although the appearance of mesas has been cited as evidence for the formation of ridges and subsequent instabilities,[7,29] sheer lack of experimental technique to examine nanoscopic thickness inhomogeneity in freestanding films has frustrated progress in the field. The shape and growth dynamics of

DOI: 10.1021/acs.langmuir.7b01871
Langmuir XXXX, XXX, XXX−XXX

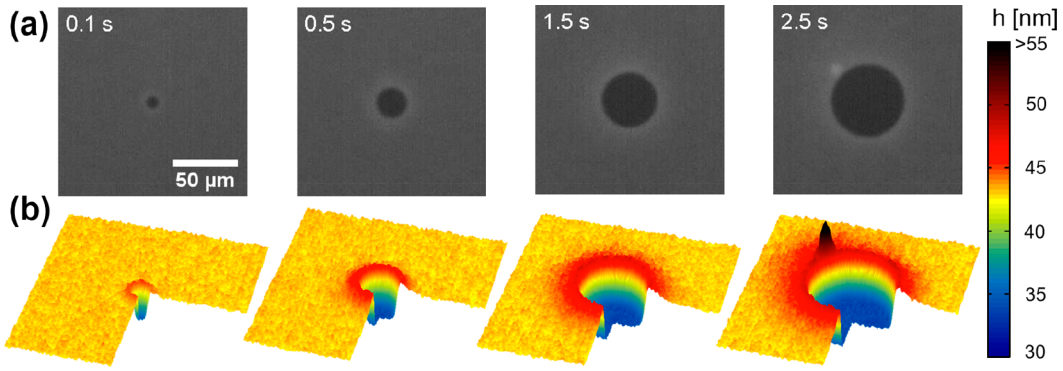

Figure 2. Domain growth and ridge formation during stratification of 50 mM SDS solution. (a) The montage with four snapshots displays the growth of a single domain during thickness transition from h_2 to h_1 under $P_c \approx 50$ Pa. (b) Thickness maps obtained using the IDIOM protocols are sliced open to highlight the cross-section of the nanoridge and the thinner domains inside. The color-map differs from Figure 1b. The formation and growth of a nanoridge flanking the expanding domain, and the emergence of thicker white spots (mesas) at a later stage (t = 2.5 s), are clearly visualized. (See Supplemental Movie online, included as Supporting Information).

nanoridges, their instabilities, and their influence on domain expansion dynamics, are neither characterized experimentally, nor mechanistically well-understood.

The techniques including surface force apparatus, fluorescence imaging, atomic force microscopy (AFM), total internal reflection microscopy, and ellipsometry typically used for characterizing nanoscopic thickness changes in supported thin films[20−23,36−40] (with at least one solid−liquid interface) are not suitable for mapping thickness variations in freestanding films. We recently demonstrated that Interferometry Digital Imaging Optical Microscopy (IDIOM) protocols[15,33] that rely on a combination of interferometry-based thickness measurement using white-light illumination and digital cameras attached to a microscope are ideal for visualizing and analyzing topographical variations in freestanding films undergoing drainage via stratification. The AFM-like thickness maps generated by IDIOM protocols allow determination of thickness variations[33] with high spatial (thickness <100 nm, lateral ∼500 nm) and temporal resolution (<1 ms). By contrast, the conventional interferometry yields the measurement of an average thickness, and stratification is manifested as stepwise thinning.[2,5,6,8,13] Furthermore, as the average thickness is computed from the reflected light intensity from a spot size of 30−60 μm in the conventional interferometry technique, it is not possible to simultaneously observe and analyze local thickness variations that accompany dynamic events like domain formation or coalescence, or the formation of nanoridges. Furthermore, with the use of high-speed cameras with frame rates exceeding 1000 Hz, fast dynamical events that had hitherto remained unobserved can be visualized, and tracked.[33] In this contribution, we show that the IDIOM protocols[15,33] enable the visualization of nanoridges and their thickness variations and transitions (see Figure 1a) in stratifying freestanding films.

Using IDIOM protocols, we present the first experimental characterization of the shape evolution of nanoridges formed near the contact line of expanding domains in stratifying, micellar films. We measure the apparent structural contribution to disjoining pressure as a function of thickness. Most significantly, we develop a self-consistent theoretical framework, a nonlinear thin film equation model that explicitly accounts for the role of supramolecular oscillatory surface forces, and describes the complex spatiotemporal evolution of nanoridges quantitatively. In this contribution, we focus on the shape and shape evolution of the nanoridge that grows at the contact line between an expanding, isolated circular domain and its thicker surrounding fim, and restrict our attention to the cases where domain growth shows the diffusive growth law $R \propto t^{1/2}$. We show that the nanoridges with asymmetric cross-sectional shape, sculpted by the supramolecular oscillatory surface forces, modulate stratification dynamics. The insights into the influence of physicochemical properties of micelle-forming surfactants, nanoparticles, self-assembling lipids, and polyelectrolytes can be used for controlling stability and lifetime of freestanding films of soft matter and colloidal dispersions in general.

RESULTS AND DISCUSSION

Measuring Disjoining Pressure Isotherms Using Thin Film Balance. Freestanding films of micellar solutions of sodium dodecyl sulfate (SDS) were formed and allowed to drain and stratify in a porous-plate thin film balance under increasing value of imposed capillary pressure P_c (see Figure 1). Drainage and stratification lead to thickness variations within the film manifested as different shades of gray (or spatial and temporal changes in intensity; see Figure 1 and Supplementary Movie online). In conventional interferometry, film thickness is computed from the average reflected light intensity obtained from a 30 to 50 μm region, by using a monochromatic light source and single photodiode for detector.[6] By contrast, the IDIOM protocols[15,33] utilize white light illumination and a large number of photodetectors within CCD or CMOS digital cameras for obtaining a pixel-wise, spatiotemporal map of intensity and consequently, of film thickness variations, as shown in Figure 1c. Careful manipulation of the imposed capillary pressure (measured using a pressure transducer) is achieved by changing the fluid volume within the thin film balance. The equilibrium film thickness of flat regions measured as a function of imposed pressure is used for generating the disjoining pressure isotherm for 50 mM (∼6 × CMC) SDS solution, as shown in Figure 1b.

For the 50 mM SDS solutions, the oscillatory nature of the supramolecular structural contribution to disjoining pressure drives stratification, leading to the four thickness steps observed for film thicknesses h < 60 nm. Experimentally, the film thickness can be accessed only when $d\Pi/dh < 0$ and $\Pi(h) = P_c \geq 30$ Pa (minimum of capillary pressure, P_c is set by the geometry of the porous plate cell), and three stable branches of

DOI: 10.1021/acs.langmuir.7b01871
Langmuir XXXX, XXX, XXX−XXX

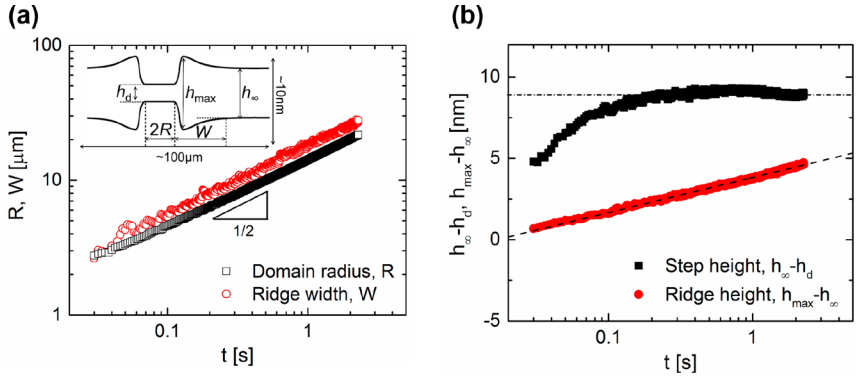

Figure 3. Domain growth and ridge evolution during stratification. (a) Time-dependent domain radius R and ridge width W, are shown in a double-logarithmic scale for 50 mM SDS solution. Both R and W scale with $t^{1/2}$ (shown as a solid line). Also included is a schematic representation of the asymmetrical ridge shape, showing a steep build-up region around the thinner domain and a relatively shallow, monotonic decay to the outside film thickness. Note that the length scale in horizontal direction is much larger than that of vertical direction. (b) Time dependence of the step height between outside film and thinner domain $h_\infty - h_d$, and the height of the ridge $h_{max} - h_\infty$, plotted on a semilogarithmic scale. The thinner domain is fully developed with a constant step height (dash dot line), after the initial fast growth. The growth of ridge height follows an apparent $h_{max} - h_\infty \propto \log t$ scaling (dashed line).

disjoining pressure are measured. At the pressure maxima of each stable branch, the film becomes unstable to thickness or pressure perturbations, and the transition to the next stable branch occurs via nucleation and growth of thinner, circular domains.

Visualizing Nanoridges Using the IDIOM Protocols. The growth of an isolated thinner domain during film stratification from thickness branch h_2 to h_1 is shown in Figure 2. The "halo" that forms around the growing domain is highlighted using contrast enhancement to the micrographs (Figure 2a) and is visualized in the thickness maps created using the IDIOM protocols (see Figure 2b). We find the flat, thin, expanding domain is flanked by a nanoridge that is thicker than the surrounding film. The nanoridge grows in both height and width over time, concomitantly with the expansion of thinner domain. At a later stage (at t = 2.5 s), topological instabilities develop within the ridge region, leading to the formation of a thicker white spot, or a nanoscopic mesa. In this study, we focus on the ridge formation growth before such instability occurs, i.e., for an axisymmetric ridge, growing at the contact line between an expanding, isolated, circular domain and its thicker surrounding.

The visualization and analysis of ridges that emerge near moving fronts (or contact lines) and their instabilities provide insights into interplay of capillarity and underlying driving forces in free surface flows.[21,22,37,38,40−43] Ridges that arise during drop impact,[42] rupture of soap films, and hydraulic jump[44] (seen in kitchen sink[44] and rinsing flows[45]) are influenced by inertia; the spreading of thin films is tempered by viscous stresses;[19,42] while disjoining pressure plays a critical role in dewetting polymer films.[21−23,40,46] The shape evolution of nanoridges or nanoscopic rims formed near the retreating contact line as holes expand within dewetting films is often characterized using AFM.[21−23,40] We show that similar nanoridges arise in stratifying micellar films, visualized for the first time in freestanding films, with these AFM-like thickness maps created by using IDIOM protocols. Remarkably, nanoridges are not reported near moving fronts in stratified films formed due to layering of small molecules[28] or supramolecular structures in lipids and smectic liquid crystal films.[16] In the following section, we analyze nanoridge growth in the constant diffusivity growth regime as it is peculiar to micellar films; a constant velocity mode is observed for domain expansion in smectic liquid crystals,[16] and for hole growth during dewetting of supported films.[19]

Nanoridge Shape and Growth. The shape evolution of the nanoridge is characterized by determining the circumferential averaged film thickness profiles, $h(r,t)$. The cross-sectional nanoridge shape is quite asymmetrical, as shown schematically in the inset of Figure 3a. In all the plots and the schematics, the film or ridge thickness is in nanometers, whereas the domain size and ridge width are in micrometers, implying that the nanoridge is quite "flat" with its lateral span (width W, in microns) nearly three orders of magnitude larger than its thickness, h (in nm). The domain radius, R, and ridge width, W, both display similar growth law $R \propto t^{1/2}$ and $W \propto t^{1/2}$ (Figure 3a). By contrast, the maximum height of the ridge $h_{max} - h_\infty \propto \log t$ shows logarithmic growth (Figure 3b). The time evolution of step height, $h_\infty - h_d$, plotted in Figure 3b, shows that the thinner domain reaches preferred thickness for applied suction pressure relatively quickly (in about 0.1 s), and thereafter no drainage flows occur within the thin domain. The ridge continues to grow axi-symmetrically until a topological instability results in the formation and growth of one or more mesas (see Figure 2). The domain expansion dynamics changes from constant apparent diffusivity to constant velocity mode after the onset of the instability.

While the diffusive growth law of isolated domains in stratified foam films has been reported before,[10,15,30] this is the first measurement of the time-evolution of nanoridge dimensions in freestanding films. The maximum thickness of the nanoridge remains small ($h_{max} - h_\infty \sim 5$ nm) in comparison to the surrounding film thickness ($h_\infty \sim 45$ nm). In contrast, the height of the nanoridges formed during dewetting is much greater than the average thin film thickness.[21,22,37−40] For ridges formed in micellar foam films, a monotonic decay of thickness into h_∞ is observed on the leeward side. In contrast, the ridges formed during dewetting of supported films are often reported (e.g., by Seemann et al.[40]) to display a thickness dip or undershoot before merging with the outside unperturbed film.

Thin Film Equation Amended with Supramolecular Oscillatory Structure Force. To better understand the shape and evolution of the ridge and describe flows within the

DOI: 10.1021/acs.langmuir.7b01871
Langmuir XXXX, XXX, XXX−XXX

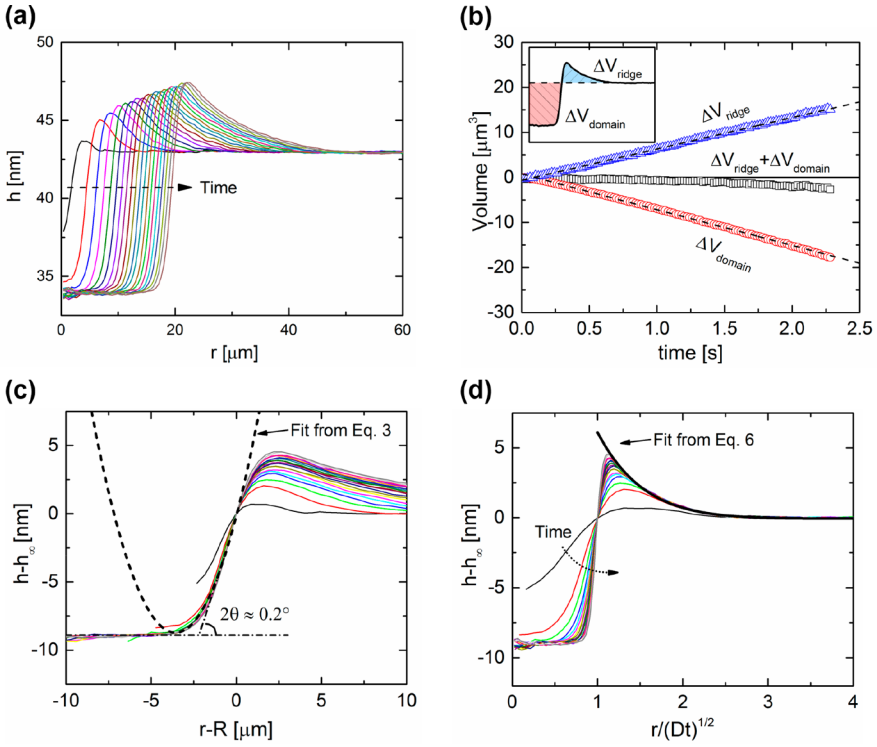

Figure 4. The shape evolution of the nanoridge formed during domain growth in stratifying foam film. (a) Time evolution of the ridge thickness profile obtained using the IDIOM protocols for 50 mM SDS solution. The time interval of successive profiles is 0.1 s. (b) Inset shows the nanoridge profile obtained experimentally at t = 1.5 s, and in color, highlights the volume drained from the domain ΔV_{domain} and the volume accumulated in the ridge ΔV_{ridge}. Since the net volume change, $(\Delta V_{domain} - \Delta V_{ridge})$, remains close to zero, ridge growth is a result of volume conservation. The slight deviation at later time could be due to slow drainage from the thin film to surrounding plateau border, or evaporation effects. (c) The build-up region in the ridge profiles, analyzed in this plot of $h - h_\infty$ versus $r - R$. By a lateral shift of the profiles, it shows that the build-up part of the ridge remains unchanged during domain growth. (d) Rescaled ridge profiles plotted as $h - h_\infty$ versus $r/(Dt)^{1/2}$. The leeward part of the profiles asymptotically approaches the same line (except ones at very initial stage t < 0.1 s). The solid black line shows the fit using eq 5 to the leeward part of the rescaled profiles.

freestanding films, we invoke here the nonlinear thin film equation derived using classical lubrication approximation to the Navier–Stokes equation. In a free-standing thin film with no-slip boundary condition on both surfaces, the following equation describes the spatial and temporal change of the film thickness:[41,43]

$$\frac{\partial h}{\partial t} + \frac{1}{r}\frac{\partial}{\partial r}\left[\frac{rh^3}{12\eta}\frac{\partial P}{\partial r}\right] = 0 \tag{1}$$

Here η is the fluid viscosity and σ is the bulk surface tension. The total pressure (called Derjaguin pressure[47]) $P = \sigma K + \Pi(h)$ includes two contributions: Laplace pressure arising from the local surface curvature, K and disjoining pressure, $\Pi(h)$ contributed by the surface forces. Since the lateral extent of the film (~100 μm) is much larger than the film thickness (~10 nm), the surface curvature can be estimated using the small slope approximation, $K \approx \frac{1}{2}\frac{d^2h}{dr^2}$. Here the prefactor of 1/2 arises as the free-standing film has two gas–liquid interfaces. Equation 1 can be written in a dimensionless form by scaling the thickness as $\bar{h} = h/h_\infty$ and the lateral dimension as $\bar{r} = r/L$, using the thickness h_∞ (in nm) of the unperturbed surrounding film and a lateral scale L (in microns). We scale the two pressure gradient terms using $(d\Pi/dh)_\infty$, i.e., from the height-derivative of disjoining pressure computed at h_∞ and the resulting nondimensional form of eq 1 is as follows:

$$\frac{\tau_S}{\tau_p}\frac{\partial \bar{h}}{\partial \bar{t}} + \frac{\tau_S}{\tau_C}\frac{1}{\bar{r}}\frac{\partial}{\partial \bar{r}}\left(\bar{r}\bar{h}^3\frac{\partial \bar{h}_{rr}}{\partial \bar{r}}\right) + \frac{1}{\bar{r}}\frac{\partial}{\partial \bar{r}}\left(\bar{r}\bar{h}^3\overline{\left(\frac{d\Pi}{dh}\right)}\frac{\partial \bar{h}}{\partial \bar{r}}\right) = 0 \tag{2}$$

Here, h_{rr} denotes the second-order derivative of film thickness, and τ_p is the process time (or the time scale of the experiment O(~seconds)). Apart from τ_p, the combination of different parameters leads to two choices for a characteristic time scale including a stretched visco-capillary time scale, $\tau_c = 24\eta h_\infty/\sigma\varepsilon^4$ typically used in describing capillary-dominated thin film flows.[41,43] Here the small parameter $\varepsilon = h_\infty/L \ll 1$ represents the ratio of the length scales in the thickness and the lateral directions. Anticipating the key role played by supramolecular oscillatory structural force contribution to disjoining pressure, we introduce here a stretched structural time $\tau_s = 12\eta/h_\infty\varepsilon^2(d\Pi/dh)_\infty$. In the following section, we compute the relative values of the relevant time scales, and discuss how the nanoridge shape is itself sculpted by the supramolecular oscillatory surface forces.

Scaling Analysis and Similarity Solutions Capture Nanoridge Shape Evolution. The asymmetric ridge profile comprises of a build-up region and a much wider leeward region (see Figure 4a), and the nanoridge volume equals the volume drained out of the expanding thinner domain (see Figure 4b). Here we aim to describe the nanoridge shape and growth as a function of time and physicochemical properties of surfactant using asymptotic solutions computed for each region. For the micellar films under investigation that show a step size

DOI: 10.1021/acs.langmuir.7b01871
Langmuir XXXX, XXX, XXX–XXX

of Δh during thinning, the typical values of the parameters are $\Delta h \approx 13$ nm, $h_\infty \approx 45$ nm, $\Pi_\infty \approx P_c \approx 50$ Pa and $\sigma \approx 35$ mN/m (determined independently by pendant drop tensiometry). As the ridge region is only slightly thicker than the surrounding equilibrium film ($h_{max} - h_\infty \leq 5$ nm as shown in Figure 3b), we use values h_∞ and Π_∞ as characteristic quantities for scaling film thickness and disjoining pressure, respectively. The gradient in disjoining pressure is estimated to be $(d\Pi/dh)_\infty \approx 4\Pi_\infty/\Delta h \approx 15$ Pa/nm. The equilibrium disjoining pressure in the surrounding film is estimated from the measured applied pressure, $\Pi_\infty \cong P_c$. An order-of-magnitude estimation of the gradient in Laplace pressure contrasted with disjoining pressure gradient (in equation leads to an intrinsic surface force-dependent length scale $L_S^2 = \sigma/2(d\Pi/dh)$. Alternatively, following Vrij[48] and others,[6,21,49] it can be shown using the linear stability analysis of thin film that the most unstable wavelength λ_c is itself proportional to $\lambda_V \propto [\sigma/2(d\Pi/dh)]^{1/2}$ or to the surface force-dependent intrinsic length-scale L_s. The ratio of two capillary and structural time scales, thus depends upon the ratio of intrinsic length-scale to the lateral scale, i.e., $\tau_s/\tau_c \approx (L_S^2/L^2)(h_\infty/\Delta h)$.

In the build-up part of the ridge, the lateral scale based on the shape of the ridge is $L \approx 1$ μm $\approx L_S$, or of the same order of magnitude as the computed value of L_S, indicating that both Laplace pressure and disjoining pressure contribute. However, the stretched structural time scale $\tau_s \sim 0.01$ s is much shorter than the process time scale of domain expansion, implying the shape of the ridge in the build-up part approaches the quasi-steady state solution. On neglecting the time-dependent $\partial h/\partial t$ term, integrating twice, and using the boundary conditions at the thinner, flat domain (i.e., within the domain radius R; see the schematic shown as inset in Figure 3a), we find that the total pressure or the Derjaguin pressure in the nonflat ridge, $\sigma K + \Pi$, is equal to the constant pressure in the flat thinner domain, Π_d. In other words, the quasi-steady solution leads to the Derjaguin equation[47] $\sigma K + \Pi = \Pi_d$, implying that the shape of the nonflat transition region is determined by the thickness-dependent disjoining pressure contribution. While a similar quasi-static profile in the transition region predicted theoretically for supported films by Joanny and deGennes for climbing uthrathin films,[50] Brochard-Wyart and Daillant for drying ultrathin films,[51] and Chuarev et al. for partially wetting ultrathin films,[47,52] the present analysis is the first instance of experimental and theoretical study of ridge shape evolution under the influence of supramolecular oscillatory surface forces in freestanding films.

The quasi-static profile for climbing, drying or partially wetting ultrathin films is determined by disjoining pressure contributed by van der Waals interactions, i.e., $\Pi_{vdW}(h) = A/6\pi h^3$, where A is the Hamaker constant.[19] Due to the relative simplicity of $\Pi_{vdW}(h)$, a single parameter, A adequately describes the quasi-static shape of the transition region, and correspondingly, shape analysis of transition region can be used for computing the thickness-dependent disjoining pressure and Hamaker constant by using the Derjaguin equation.[47] We postulate that the iterated analysis of the build-up region of ridges formed at each of the progressive stepwise thinning transitions could be used for evaluating the disjoining pressure $\Pi(h)$ contributed by supramolecular oscillatory structural forces, and contrasting with the measured value. Leaving such analysis for a future study, in the present article, we will focus on the hydrodynamic processes that drive ridge evolution, and the overall stratification kinetics. The complexities and challenges associated with fluid−substrate interactions and slip near the contact line that arise in dewetting and spreading studies,[19,21−24,37−43,46,47] are absent from the flows underlying domain expansion and ridge growth in micellar freestanding films, enabling the analysis and simplifications that follow.

Using the Derjaguin equation $\sigma K + \Pi = \Pi_d$, and rewriting the curvature term in small slope limit as $K \approx \frac{1}{2}\frac{d^2h}{dr^2} = \frac{1}{2}h_{rr}$, leads to a second-order differential equation. Using $h = h_d$ and $h' = 0$ in the flat domain, recalling $(d\Pi/dh)_\infty \approx 4\Pi_\infty/\Delta h$ and the intrinsic structural force length-scale, L_s, leads to the following expression for the thickness in the build-up region:

$$h - h_d \approx \frac{\Delta h}{16 L_s^2}(r - R)^2 \tag{3}$$

The transition from the thinner domain of thickness, h_d, to the peak of the ridge at thickness, h_{max} in the build-up region is relatively steep when contrasted with the shallower slope observed in transition from the ridge peak to the outside film thickness, h_∞ in the leeward region (Figure 4a). In accordance with this quasi-steady state solution, the ridge profiles overlap in the build-up part in the comoving frame of reference, i.e., when $h - h_\infty$ is plotted as a function of $r - R(t)$ as shown in Figure 4c. The thickness profile in the build-up part maintains a constant contact angle with the thinner domain, measured to be $2\theta = 0.2 \pm 0.1°$ (implying that the small slope limit is fully justified here). The parabolic profile obtained in eq 4 describes the ridge shape in the build-up region reasonably well.

In contrast to the build-up region, due to a larger length-scale on the wider leeward side of the ridge, $L \gg L_S$, the Laplace pressure term drops out (as $\tau_s/\tau_c \ll 1$) from eq 2. Thus, the dynamics are primarily controlled by the disjoining pressure gradient. On using $L = 20$ μm, the estimated characteristic stretched structural time scale $\tau_s \sim O(10^2$ s) becomes comparable to the process time, and therefore the time-dependent effects are retained. In the dimensional version, the dynamics in the leeward region are governed by the following equation:

$$\frac{\partial h}{\partial t} + \frac{1}{r}\frac{\partial}{\partial r}\left(r\frac{h^3}{12\eta}\frac{d\Pi}{dh}\frac{\partial h}{\partial r}\right) = 0 \tag{4}$$

This equation can be treated as a two-dimensional diffusion equation with an effective diffusivity defined as

$$D_{eff} = -\frac{h^3}{12\eta}\frac{d\Pi}{dh} \tag{5}$$

which depends on the thickness profile of the ridge, and the disjoining pressure isotherm. The thin film equation, also known as the "height diffusion" equation (see Supporting Information for detailed derivation), creates a self-similar thickness profile $h(r,t) - h_\infty = f(r/t^{1/2})$. Thus, the width of the nanoridge, W is expected to grow with $W \propto t^{1/2}$ scaling, following a diffusive growth law, which is also followed by the radius of expanding domain, $R \propto t^{1/2}$.

The self-similar nature of the leeward ridge profile is evident in the plot of thickness $h - h_\infty$ versus $r/(Dt)^{1/2}$ as shown in Figure 4d. Here $D = dR^2/dt$ is the areal growth rate of the thinner domain radius that can be measured experimentally. Deviation occurs in the very early stage ($t < 0.1$s) as the thinner domain is still far from its metastable thickness (see Figure 3b). Effectively, the outward flux of thickness $\Delta h(dR/dt)$ is controlled by the outward flux $D_{eff}(dh/dr)$from the nanoridge.

DOI: 10.1021/acs.langmuir.7b01871
Langmuir XXXX, XXX, XXX−XXX

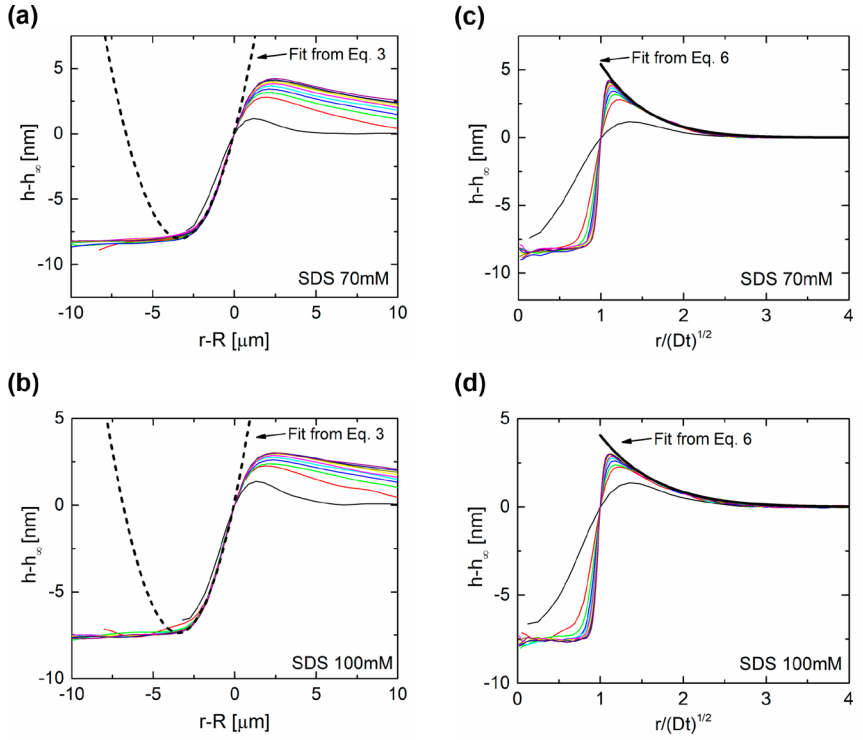

Figure 5. The ridge evolution in stratifying film made with 70 mM and 100 mM SDS solution. (a,b) The time-independent, quasi-steady shape of the ridge in the build-up region are shown here for 70 mM and 100 mM SDS solutions, respectively. The $h - h_\infty$ versus $r - R$ plots all collapse into a parabolic shape (see eq 3). (c,d) The self-similar shape of the leeward part of the ridge is shown for 70 mM and 100 mM SDS solutions respectively, by plotting thickness against similarity variable $r/(Dt^{1/2})$. Also shown is the fit to the asymptotic solution (see eq 6).

Equating the two fluxes shows that $dR/dt \propto D_{eff}/W$, that is, the domain growth is expected to display a constant diffusivity regime $R \sim D_{eff}t^{1/2}$, in agreement with the experimental results in Figure 3a.

An analytical solution to eq 4 can be written down by making the zeroth order approximation to the diffusivity, i.e., $D_{eff} \approx D_{eff}(h_\infty) = \frac{h_\infty^3}{12\eta}\frac{d\Pi}{dh}\Big|_{h=h_\infty}$. The similarity solution for the leeward profile is as follows:

$$h(r/R) - h_\infty = -\frac{h_\infty - h_d}{\mathrm{Ei}(-c) + e^{-c}/c}\mathrm{Ei}\left(-\frac{r^2}{4D_{eff}t}\right) \quad (6)$$

where $\mathrm{Ei}(x) = -\int_{-x}^{\infty}\frac{e^{-u}}{u}du$ is the exponential integral function. The height difference between the surrounding domain and the thinner domain, $h_\infty - h_d$ becomes constant after t = 0.1 s (Figure 3b). Here $c = R^2/4D_{eff}t = D/4D_{eff}$ is the ratio of areal growth rate and effective apparent diffusivity (both depend on surfactant concentration). While the thickness profile in the leeward region (eq 6) was anticipated by a theoretical analysis carried out by Heinig, Beltrán, and Langevin[31] for thin films formed with polyelectrolyte−surfactant mixtures, our approach allows a clearer and more comprehensive determination of nanoridge profiles in both the leeward and the build-up regions. Quantitative agreement with the experimentally obtained value is observed when height profile in eq 6 (solid black line fit in Figure 4d) is plotted using the experimental values of $h_\infty - h_d$ = 9.0 nm, D = 206 $\mu m^2/s$, (obtained from data shown in Figures 3−4) and by setting c as a fitting parameter. The estimated value of $c \sim 0.52$ is comparable to c = 0.35 obtained from the fit.

Nanoridge shape evolution was visualized and characterization using multiple movies of SDS solutions undergoing stratification, using solutions in the concentration range from 30 mM < c < 100 mM. We find that the data presented for 50 mM SDS solutions is quite representative of the nanoridge shape and shape evolution, as can be illustrated by additional data shown in Figure 5. The ridge thickness profiles obtained for 70 mM and 100 mM SDS are remarkably similar to the results from 50 mM SDS (see Figure 4 for comparison). The build-up part of the ridge can be described quantitatively by the quasi-steady solution in the moving frame of $r - R(t)$, while the leeward part of the ridge for both concentrations exhibits the self-similar decay in height away from the peak of the ridge. In Figure 5c,d), the scaled ridge profiles appear to be fit quite well by the asymptotic solution given in eq 6. The values of fitting parameter, c obtained are 0.36 for 70 mM, and 0.29 for 100 mM, respectively. Though, both domain growth rate D and effective diffusivity D_{eff} increase with an increase in concentration, the ratio of the two, $c = D/4D_{eff}$, seems to remain relatively constant.

The asymptotic, approximate solutions that describe the nanoridge shape in build-up and leeward regions (as shown in Figure 4 and Figure 5) highlight the power of thin film equation, scaling theory, and similarity solutions in providing insights into the underlying physics. Furthermore, for small $r^2/4D_{eff}t \ll 1$, a series expansion for the Ei function can be written out to show that for the region near the peak of the ridge, the thickness evolution exhibits a dependence $h \propto \log t$, as observed experimentally (shown in Figure 3b). We have verified that a numerical solution of the thin film equation (eq 2) with supramolecular oscillatory structural force contribution added, results in an asymmetric ridge shape, and these results

DOI: 10.1021/acs.langmuir.7b01871
Langmuir XXXX, XXX, XXX−XXX

will be detailed in a future paper. The shape of the nanoridge thus is a consequence of the influence of supramolecular oscillatory surface forces, and, in contrast to ridges formed in dewetting or drying polymeric films,[21−24,40] neither slip nor viscoelasticity plays any role.

CONCLUSIONS

In summary, we show that the domain expansion dynamics and stratification kinetics are modulated by the fluxes and flows through nanoridges that are spontaneously formed at the moving front between expanding thinner domain and the thicker surrounding film. The experimental and theoretical investigation of nanoridge formation and growth presented here highlights the role played by the supramolecular oscillatory surface forces in defining the nanoscopic topography, thicknesss transitions, and overall lifetime of micellar foam films. While flat regions with discretely different thicknesses can coexist as due to the oscillatory nature of the disjoining pressure, both the curvature-dependent Laplace pressure and the thickness-dependent disjoining pressure contribute to the shape and the shape evolution of the nonflat structures, including ridges. The shape and shape evolution of the nanoridge growing at the contact line between an expanding, isolated, circular domain and its thicker surrounding, such that domain radius shows diffusive growth $R \propto t^{1/2}$ are analyzed in this study. We show that a similar diffusive growth law $W \propto t^{1/2}$ is displayed by the nanoridge width, and the height of the ridge shows a milder, logarithmic growth $h_{max} - h_{min} \propto \log t$. We show that the shape of the nanoridge is asymmetric and the ridge profile comprises of a build-up region and a much wider leeward region. We show that the nanoridge volume equals the volume drained out of the expanding thinner domain, thus implying that the ridge formation is a manifestation of local volume conversation.

We show that the model based on nonlinear thin film equation amended with supramolecular oscillatory surface forces provides a self-consistent description of domain growth, nanoridge formation, as well as the influence of both hydrodynamic and thermodynamic parameters underlying stratification. In particular, we derive a similarity solution to quantitatively describe the self-similar ridge profile in the leeward region. In contrast to the leeward region where the ridge profiles extracted using IDIOM overlap when the thickness $h - h_\infty$ is plotted as a function of the similarity variable $r/(Dt)^{1/2}$, the ridge profile in the build-up region overlap when the thickness $h - h_\infty$ is plotted as a function of $r - R(t)$. The thickness profile in the build-up part maintains a constant contact angle with the thinner domain, measured to be $2\theta = 0.2 \pm 0.1°$, thus implying that the small slope approximation for evaluating curvature and lubrication approximation for thin film flow are fully justified here. We show that the ridge profile in build-up region are captured well by a quasi-static solution based on the Derjaguin equation, and can be fit by a parabolic shape as $h - h_d \propto (r - R)^2$. As the physicochemical properties of micelle-forming surfactants, nanoparticles, self-assembling lipids, and polyelectrolyte−surfactant complexes determine surface tension, supramolecular oscillatory surface force, and solution viscosity, the theoretical analysis described herein can be used for predicting and controlling stability and lifetime of freestanding films in colloidal dispersions including foams and emulsions. We anticipate that a widespread use of the IDIOM protocols and the theoretical analysis developed and described here will enable a deeper understanding of the influence of charge, chemical structure (of surfactant, polyelectrolytes, or lipids) and confinement-induced structuring on thermodynamics and hydrodynamics of stratifying freestanding films, and soft materials.

MATERIALS AND METHODS

Materials. The foam films are prepared with solutions of sodium dodecyl sulfate (SDS) above the critical micelle concentration (CMC). SDS (Sigma-Aldrich Co., St. Louis, MO, L6026, > 99.0%) is used without further purification. The CMC of SDS is measured with maximum bubble pressure tensiometry and pendant drop tensiometry to be 8.2 mM, which is consistent with the values reported in the literature[53,54] (8 mM-10 mM at 25 °C), and the smooth transition at CMC shows that the as-made solutions of as-received SDS are relatively free of impurities.[53] All solutions are prepared with deionized water with resistivity of 18.2 MΩ without addition of electrolytes.

Thin Film Balance. Thin film experiments are carried out in a porous-plate type thin film balance[12,55] (see Figure 1a). The cell used in this study is made from fritted glass disk (Wilmad-LabGlass) with porosity of 10−15 μm. The cell geometry is shown in Figure 1a. The hole at the center of the disk is drilled with 1 mm diamond drill bit, and tapered with a spherical grinding head. The disk thickness around the hole is reduced to ∼0.1 mm. This geometry permits formation of foam film with very low applied pressure (∼30 Pa), which is beneficial for probing meta-stability of higher thickness branches in stratifying foam films. The porous plate cell is connected through Teflon tubing to a pressure transducer (Omega, PX409−001G5 V) and syringe pump (New Era NE-1000), and placed in a closed container, in which air is saturated with the same solution to minimize the effect of evaporation. The foam film is formed by withdrawing liquid from the presoaked porous plate. The pressure applied to the foam film depends on the volume of liquid removed, which is controlled by the syringe pump. The pressure sensor is calibrated following the procedure described by Dimitrova et al.[55]

The foam film is visualized by using a reflected light microscope assembly that consist of precision microscope lens system (Navitar Zoom 6000) and a high-resolution, high speed color camera (FASTCAM Mini UX100). Illumination is provided by a white LED light source (Fiilex P360EX, color temperature set to 5100K).

Thickness Determination. The IDIOM protocols used for film thickness mapping h (x,y,t) are based on measurement of spatiotemporal variation in interference intensity $I(x,y,t)$ and utilize the in-built photosensor array of a digital camera.[15,33] Every pixel in a color image obtained by a digital camera can be read as a composite of three intensities of red (wavelength λ = 650 nm), green (λ = 546 nm), and blue (λ = 470 nm) light, and each color channel has values in the range of 0−4095 (for RAW image with 12-bit depth). The IDIOM protocols rely on white light illumination and use digital filtering to obtain simultaneous intensity maps and consequently thickness measurements by using the interferometry equation:

$$h = \left(\frac{\lambda}{2n\pi}\right) \arcsin\left(\sqrt{\frac{\Delta}{1 + 4R(1-\Delta)/(1-R)^2}}\right) \quad (7)$$

where λ is the wavelength of light, $\Delta = (I - I_{min})/(I_{max} - I_{min})$, and $R = (n-1)^2/(n+1)^2$. Here I is the intensity value measured in each pixel, I_{max} and I_{min} are maxima and minima intensities of interference, and n is the refractive index of the bulk solution (here n = 1.33). The image analysis is carried out in MATLAB R2015a with specially developed codes. Thickness measured separately from each of the three color channels is found to be in good agreement (<1 nm difference). The IDIOM technique allows us to map the thickness of the entire film area. With the aforementioned microscope assembly, the thickness measurement reaches a spatial resolution of 0.55 μm/pixel, thickness resolution of ∼1 nm, and under a millisecond temporal resolution.

DOI: 10.1021/acs.langmuir.7b01871
Langmuir XXXX, XXX, XXX−XXX

■ ASSOCIATED CONTENT

Supporting Information

The Supporting Information is available free of charge on the ACS Publications website at DOI: 10.1021/acs.langmuir.7b01871.

Similarity solution in the leeward part of the nanoridge, and additional data on ridge formation and evolution (PDF)

Thickness map during domain expansion in stratifying foam film made with 50 mM SDS (AVI)

■ AUTHOR INFORMATION

Corresponding Author

*E-mail: viveks@uic.edu.

ORCID

Vivek Sharma: 0000-0003-1152-1285

Notes

The authors declare no competing financial interest.

■ ACKNOWLEDGMENTS

Y.Z. carried out the experiments and theoretical analysis under the supervision of V.S. Y.Z. and V.S. cowrote the manuscript. Extended discussions with Subinuer Yilixiati on the supramolecular oscillatory surface force contributions and stratification dynamics, and with Prerana Rathore on ridge shape evolution are acknowledged.

■ REFERENCES

(1) Boys, C. V. *Soap Bubbles: Their Colours and the Forces Which Mold Them.*; Society for Promoting Christian Knowledge: London, 1912; Vol. *542*.

(2) Bergeron, V. Forces and Structure in Thin Liquid Soap Films. *J. Phys.: Condens. Matter* **1999**, *11*, R215−R238.

(3) Cantat, I.; Cohen-Addad, S.; Elias, F.; Graner, F.; Höhler, R.; Pitois, O. *Foams: Structure and Dynamics*; Oxford University Press: Oxford, 2013.

(4) Mysels, K. J.; Frankel, S.; Shinoda, K. *Soap Films: Studies of Their Thinning and a Bibliography*; Pergamon Press: Oxford, 1959.

(5) Exerowa, D.; Kruglyakov, P. M. *Foam and Foam Films: Theory, Experiment, Application*; Elsevier: Amsterdam, 1997; Vol. *5*.

(6) Sheludko, A. Thin Liquid Films. *Adv. Colloid Interface Sci.* **1967**, *1*, 391−464.

(7) Langevin, D.; Sonin, A. A. Thinning of Soap Films. *Adv. Colloid Interface Sci.* **1994**, *51*, 1−27.

(8) Nikolov, A. D.; Wasan, D. T.; Kralchevsky, P. A.; Ivanov, I. B. Ordered Structures in Thinning Micellar Foam and Latex Films. *Yamada Conference Proceedings on Ordering and Organisation in Ionic Solutions, Kyoto, Japan*: Ise, N., Sogami, I., Eds.; World Scientific: Singapore, 1988; pp 302−414.

(9) Nikolov, A. D.; Kralchevsky, P. A.; Ivanov, I. B.; Wasan, D. T. Ordered Micelle Structuring in Thin Films Formed from Anionic Surfactant Solutions: Ii. Model Development. *J. Colloid Interface Sci.* **1989**, *133*, 13−22.

(10) Kralchevski, P. A.; Nikolov, A. D.; Wasan, D. T.; Ivanov, I. B. Formation and Expansion of Dark Spots in Stratifying Foam Films. *Langmuir* **1990**, *6*, 1180−1189.

(11) Wasan, D. T.; Nikolov, A. D. Thin Liquid Films Containing Micelles or Nanoparticles. *Curr. Opin. Colloid Interface Sci.* **2008**, *13*, 128−133.

(12) Bergeron, V.; Radke, C. J. Equilibrium Measurements of Oscillatory Disjoining Pressures in Aqueous Foam Films. *Langmuir* **1992**, *8*, 3020−3026.

(13) Bergeron, V.; Radke, C. J. Disjoining Pressure and Stratification in Asymmetric Thin-Liquid Films. *Colloid Polym. Sci.* **1995**, *273*, 165−174.

(14) von Klitzing, R.; Thormann, E.; Nylander, T.; Langevin, D.; Stubenrauch, C. Confinement of Linear Polymers, Surfactants, and Particles between Interfaces. *Adv. Colloid Interface Sci.* **2010**, *155*, 19−31.

(15) Zhang, Y.; Sharma, V. Domain Expansion Dynamics in Stratifying Foam Films: Experiments. *Soft Matter* **2015**, *11*, 4408−4417.

(16) Oswald, P.; Pieranski, P. *Smectic and Columnar Liquid Crystals: Concepts and Physical Properties Illustrated by Experiments*; CRC Press: Boca Raton, FL, 2005.

(17) Sethumadhavan, G. N.; Nikolov, A.; Wasan, D. Film Stratification in the Presence of Colloidal Particles. *Langmuir* **2001**, *17*, 2059−2062.

(18) Derjaguin, B. V.; Churaev, N. V.; Muller, V. M. *Surface Forces*; Springer: New York, 1987.

(19) de Gennes, P. G.; Brochard-Wyart, F.; Quéré, D. *Capillarity and Wetting Phenomena: Drops, Bubbles, Pearls, Waves*; Springer: New York, 2004.

(20) Israelachvili, J. N. *Intermolecular and Surface Forces*, 3rd ed.; Academic Press: Cambridge, MA, 2011.

(21) Kalliadasis, S.; Thiele, U. *Thin Films of Soft Matter*; Springer: Wien/New York, 2007.

(22) Blossey, R. *Thin Liquid Films: Dewetting and Polymer Flow*. Springer: New York, 2012.

(23) Mukherjee, R.; Sharma, A. Instability, Self-Organization and Pattern Formation in Thin Soft Films. *Soft Matter* **2015**, *11*, 8717−8740.

(24) Popescu, M. N.; Oshanin, G.; Dietrich, S.; Cazabat, A. M. Precursor Films in Wetting Phenomena. *J. Phys.: Condens. Matter* **2012**, *24*, 243102.

(25) Fennell Evans, D.; Wennerström, H. *The Colloidal Domain: Where Physics, Chemistry, Biology, and Technology Meet*, 2nd ed.; Wiley-VCH: New York, 1999.

(26) Johonnott, E. S. LXVIII. The Black Spot in Thin Liquid Films. *Philos. Mag.* **1906**, *11*, 746−753.

(27) Perrin, J. La Stratification Des Lames Liquides. *Ann. Phys. (Paris, Fr.)* **1918**, *9*, 160−184.

(28) Heslot, F.; Fraysse, N.; Cazabat, A. M. Molecular Layering in the Spreading of Wetting Liquid Drops. *Nature* **1989**, *338*, 640−642.

(29) Bergeron, V.; Jimenez-Laguna, A. I.; Radke, C. J. Hole Formation and Sheeting in the Drainage of Thin Liquid Films. *Langmuir* **1992**, *8*, 3027−3032.

(30) Beltran, C. M.; Langevin, D. Stratification Kinetics of Polyelectrolyte Solutions Confined in Thin Films. *Phys. Rev. Lett.* **2005**, *94*, 217803.

(31) Heinig, P.; Márquez Beltrán, C. M.; Langevin, D. Domain Growth Dynamics and Local Viscosity in Stratifying Foam Films. *Phys. Rev. E* **2006**, *73*, 051607.

(32) Lee, J.; Nikolov, A.; Wasan, D. Stratification of a Foam Film Formed from a Nonionic Micellar Solution: Experiments and Modeling. *Langmuir* **2016**, *32*, 4837−4847.

(33) Zhang, Y.; Yilixiati, S.; Pearsall, C.; Sharma, V. Nanoscopic Terraces, Mesas, and Ridges in Freely Standing Thin Films Sculpted by Supramolecular Oscillatory Surface Forces. *ACS Nano* **2016**, *10*, 4678−4683.

(34) Sonin, A.; Bonfillon, A.; Langevin, D. Thinning of Soap Films: The Role of Surface Viscoelasticity. *J. Colloid Interface Sci.* **1994**, *162*, 323−330.

(35) Sonin, A.; Langevin, D. Stratification Dynamics of Thin Films Made from Aqueous Micellar Solutions. *EPL (Europhysics Letters)* **1993**, *22*, 271.

(36) Butt, H.-J.; Cappella, B.; Kappl, M. Force Measurements with the Atomic Force Microscope: Technique, Interpretation and Applications. *Surf. Sci. Rep.* **2005**, *59*, 1−152.

(37) Seemann, R.; Herminghaus, S.; Jacobs, K. Dewetting Patterns and Molecular Forces: A Reconciliation. *Phys. Rev. Lett.* **2001**, *86*, 5534.

(38) Seemann, R.; Herminghaus, S.; Neto, C.; Schlagowski, S.; Podzimek, D.; Konrad, R.; Mantz, H.; Jacobs, K. Dynamics and

DOI: 10.1021/acs.langmuir.7b01871
Langmuir XXXX, XXX, XXX−XXX

Structure Formation in Thin Polymer Melt Films. *J. Phys.: Condens. Matter* **2005**, *17*, S267.
(39) Reiter, G.; Al Akhrass, S.; Hamieh, M.; Damman, P.; Gabriele, S.; Vilmin, T.; Raphaël, E. Dewetting as an Investigative Tool for Studying Properties of Thin Polymer Films. *Eur. Phys. J.: Spec. Top.* **2009**, *166*, 165−172.
(40) Seemann, R.; Herminghaus, S.; Jacobs, K. Shape of a Liquid Front Upon Dewetting. *Phys. Rev. Lett.* **2001**, *87*, 196101.
(41) Oron, A.; Davis, S. H.; Bankoff, S. G. Long-Scale Evolution of Thin Liquid Films. *Rev. Mod. Phys.* **1997**, *69*, 931.
(42) Yarin, A. L. Drop Impact Dynamics: Splashing, Spreading, Receding, Bouncing. *Annu. Rev. Fluid Mech.* **2006**, *38*, 159−192.
(43) Craster, R. V.; Matar, O. K. Dynamics and Stability of Thin Liquid Films. *Rev. Mod. Phys.* **2009**, *81*, 1131−1198.
(44) Bush, J. W. M.; Aristoff, J. M.; Hosoi, A. E. An Experimental Investigation of the Stability of the Circular Hydraulic Jump. *J. Fluid Mech.* **2006**, *558*, 33−52.
(45) Walker, T. W.; Hsu, T. T.; Frank, C. W.; Fuller, G. G. Role of Shear-Thinning on the Dynamics of Rinsing Flow by an Impinging Jet. *Phys. Fluids* **2012**, *24*, 093102.
(46) Becker, J.; Grün, G.; Seemann, R.; Mantz, H.; Jacobs, K.; Mecke, K. R.; Blossey, R. Complex Dewetting Scenarios Captured by Thin-Film Models. *Nat. Mater.* **2003**, *2*, 59−63.
(47) Starov, V. M.; Velarde, M. G.; Radke, C. J. *Wetting and Spreading Dynamics*; CRC Press: New York, 2007.
(48) Vrij, A. Possible Mechanism for Spontaneous Rupture of Thin Free Liquid Films. *Discuss. Faraday Soc.* **1966**, *42*, 23−33.
(49) Thiele, U. Thin Film Evolution Equations from (Evaporating) Dewetting Liquid Layers to Epitaxial Growth. *J. Phys.: Condens. Matter* **2010**, *22*, 084019.
(50) Joanny, J. F.; De Gennes, P.-G. Upward Creep of a Wetting Fluid: A Scaling Analysis. *J. Phys. (Paris)* **1986**, *47*, 121−127.
(51) Brochard-Wyart, F.; Daillant, J. Drying of Solids Wetted by Thin Liquid Films. *Can. J. Phys.* **1990**, *68*, 1084−1088.
(52) Churaev, N. V.; Starov, V. M.; Derjaguin, B. V. The Shape of the Transition Zone between a Thin Film and Bulk Liquid and the Line Tension. *J. Colloid Interface Sci.* **1982**, *89*, 16−24.
(53) Mysels, K. J. Surface Tension of Solutions of Pure Sodium Dodecyl Sulfate. *Langmuir* **1986**, *2*, 423−428.
(54) Rosen, M. J.; Kunjappu, J. T. *Surfactants and Interfacial Phenomena*, 4th ed.; John Wiley & Sons: Hoboken, NJ, 2012.
(55) Dimitrova, T. D.; Leal-Calderon, F.; Gurkov, T. D.; Campbell, B. Disjoining Pressure Vs Thickness Isotherms of Thin Emulsion Films Stabilized by Proteins. *Langmuir* **2001**, *17*, 8069−8077.

DOI: 10.1021/acs.langmuir.7b01871
Langmuir XXXX, XXX, XXX−XXX